

# Observation of Diboson Production in a Semileptonic Decay at CDF

M. Hurwitz, on behalf of the CDF Collaboration

Enrico Fermi Institute, University of Chicago, Chicago, IL 60637, USA

We present the first observation of  $WW + WZ$  production in the channel with an identified lepton and two jets in  $2.7 \text{ fb}^{-1}$  of integrated luminosity collected with the CDF II detector in  $p\bar{p}$  collisions at  $\sqrt{s} = 1.96 \text{ TeV}$ . The signal is separated from the large background using matrix element calculations and is observed with a significance of  $5.4\sigma$ . The  $WW + WZ$  production cross section is measured to be  $17.7 \pm 3.1(\text{stat}) \pm 2.4(\text{sys}) \text{ pb}$ , in good agreement with standard model predictions. A complimentary measurement using a fit to the dijet mass is also presented.

## 1. Introduction

Measurements of heavy vector boson pairs ( $WW$ ,  $WZ$ , and  $ZZ$ ) are important tests of the electroweak sector of the Standard Model (SM). Deviations of the production cross section from SM predictions could indicate the presence of new particles or interactions [1]. Furthermore the topology of diboson events is similar to events where a Higgs boson is produced in association with a  $W$  or a  $Z$ , so diboson searches and measurements are useful tests of analysis strategies employed in Higgs searches.

$WW$  and  $WZ$  production has been observed at the Tevatron in channels where both bosons decay leptonically [2] [3]. In semi-leptonic modes, where one boson decays to two quarks, large backgrounds make the signal extraction more challenging. CDF recently reported the first observation of such semi-leptonic decays in a channel with two jets and large missing transverse energy [4]. We present observation of semi-leptonic diboson decays in a channel with an identified lepton and two jets. The D0 collaboration has previously reported evidence of this signal in  $1.07 \text{ fb}^{-1}$  [5].

Discrimination of the signal processes from the large backgrounds is accomplished by use of matrix element probabilities. The implementation of this search technique follows that used in the search for associated Higgs boson production [6]. A second complimentary technique fits the invariant mass of the two-jet system (referred to as the dijet mass or  $M_{jj}$ ).

## 2. Experimental Apparatus

The production is observed in  $2.7 \text{ fb}^{-1}$  of  $p\bar{p}$  collision data with  $\sqrt{s} = 1.96 \text{ TeV}$  collected by the CDF II detector, which is described in detail elsewhere [7]. The aspects of the detector relevant to this analysis are described here briefly. The tracking system is composed of silicon microstrip detectors and open-cell drift chambers inside of a 1.4 T solenoid. Electromagnetic lead-scintillator and hadronic iron-scintillator sampling calorimeters segmented in a projective geometry surround the tracking. The central calorimeter covers  $|\eta| < 1.1$  while the plug calorimeters extend

the calorimetry into the region  $1.1 < |\eta| < 3.6$ . Outside of the calorimeter are muon detectors composed of scintillators and drift chambers. Cherenkov counters around the beam pipe and in the plug calorimeter count the inelastic collisions per bunch crossing and provide the luminosity measurement.

We use a cylindrical coordinate system with its origin in the center of the detector, where  $\theta$  and  $\phi$  are the polar and azimuthal angles, respectively, and pseudorapidity is  $\eta = -\ln \tan(\theta/2)$ . The missing  $E_T$  ( $\cancel{E}_T$ ) is defined by  $\cancel{E}_T = -\sum_i E_T^i \hat{n}_i$ ,  $i$  = calorimeter tower number, where  $\hat{n}_i$  is a unit vector perpendicular to the beam axis and pointing to the  $i^{\text{th}}$  calorimeter tower.  $\cancel{E}_T$  is corrected for high-energy muons and jet energy corrections. We define the missing transverse energy  $\cancel{E}_T = |\cancel{E}_T|$ . The transverse momentum  $p_T$  is defined to be  $p \sin \theta$ .

## 3. Event Selection

The data samples used in this analysis are collected using trigger paths requiring a central electron (muon) with  $E_T(p_T) > 18 \text{ GeV}$  as well as a trigger path requiring two jets and large  $\cancel{E}_T$ . Offline we further select events by requiring an electron or muon candidate with  $p_T > 20 \text{ GeV}$  and exactly two jets with  $E_T > 25 \text{ GeV}$ . Jets are clustered using a fixed-cone algorithm with radius  $\Delta R = \sqrt{(\Delta\eta)^2 + (\Delta\phi)^2} = 0.4$  and their energies are corrected for detector effects.

Several event vetos are imposed to reduce background levels and achieve good agreement between data and simulation. We reject events with any additional jets with  $E_T > 12 \text{ GeV}$ . We reduce the backgrounds due to fully leptonic decays of  $t\bar{t}$  and diboson events by vetoing on additional charged leptons. We also reject events containing dilepton pairs consistent with decay from a  $Z$  boson, where the second lepton passes very loose identification cuts. Cosmic ray and photon conversion vetos are implemented.

We impose additional requirements to reduce the level of background due to QCD multi-jet events. These events will enter our sample if a jet fakes an electron or muon and mismeasurement leads to large

$\cancel{E}_T$ . QCD multi-jet events are difficult to model, so we reduce their contribution as much as possible. In events with a muon, we require  $\cancel{E}_T > 20$  GeV and  $m_T(W) > 10$  GeV, where  $m_T(W)$  is the transverse mass of the lepton- $\cancel{E}_T$  system. Jets are more likely to fake an electron than a muon, so we impose particularly strict requirements in events with an electron, requiring  $\cancel{E}_T > 40$  GeV and  $m_T(W) > 70$  GeV, as well as placing requirements on the  $\cancel{E}_T$  significance and the angle between the  $\cancel{E}_T$  and the second jet.

## 4. Modeling and Backgrounds

The dominant background to the diboson signal is  $W$ +jets production where the  $W$  decays leptonically. Smaller but non-negligible backgrounds come from QCD multijet,  $Z$ +jet,  $t\bar{t}$ , and single top production. The modeling for all processes except QCD multijet events is provided by event generators and a GEANT-based CDFII detector simulation. PYTHIA is used to model  $WW$ ,  $WZ$ , and  $t\bar{t}$  [8] events. The  $W/Z$ +jets backgrounds are modeled using the fixed-order generator ALPGEN interfaced with the PYTHIA parton showering framework [9]. MADEVENT interfaced with PYTHIA is used for the single top background [10]. The QCD background is modeled using data events passing loosened lepton requirements.

The normalization of  $WW$ ,  $WZ$ ,  $Z$ +jets,  $t\bar{t}$ , and single top backgrounds is estimated using predicted or (in the case of  $Z$ +jets) measured cross sections and efficiencies derived from simulation. The normalization of the QCD background is estimated by fitting the  $\cancel{E}_T$  spectrum in data to the sum of all contributing processes, where the QCD and  $W$ +jets normalizations float in the fit. While this fit provides an initial estimate of the  $W$ +jets normalization, this normalization is a free parameter in the final fit used to extract the diboson cross section. The expected event yields are shown in Table I. The observed yield agrees well with the total expected yield since the predicted yields are derived from a fit to the data.

Table I Expected event yields for signal and background processes and total observed number of events.

Process	Event yield
$WW$ signal	$446 \pm 17$
$WZ$ signal	$79 \pm 3$
$W$ +jets	$10175 \pm 152$
$Z$ +jets	$584 \pm 43$
QCD multijet	$283 \pm 113$
$t\bar{t}$	$131 \pm 9$
single top	$110 \pm 8$
Observed	11812

We expect 525 signal events out of 11812 total events. The dominant background is due to  $W$ +jet events. The QCD multi-jet background is small due to the stringent cuts imposed to reduce its size.

## 5. Matrix Element Methodology

A matrix element method is employed to separate signal and background events. The probability that an event was produced by a given process is determined using the leading-order differential cross section for that process. For an event with measured quantities  $x$ , we integrate the appropriate differential cross section  $d\sigma(y)$  over the partonic quantities  $y$  convolved with the parton distribution functions (PDFs),  $f(y_1)$ ,  $f(y_2)$ , and over transfer functions describing detector resolution effects,  $W(y, x)$ :

$$P(x) = \frac{1}{\sigma} \int d\sigma(y) dq_1 dq_2 f(y_1) f(y_2) W(y, x). \quad (1)$$

We use the CTEQ5L PDF parameterization [11]. The lepton momenta and jet angles are assumed to be measured exactly.  $W(x, y)$  is a mapping of measured jet energy to partonic energy derived using the full detector simulation. The integration is performed over the energy of the partons and  $p_z^y$ . The matrix element is calculated with tree-level diagrams from MADGRAPH [12]. Event probability densities are calculated for the signal processes  $WW$  and  $WZ$ , as well as for the  $Wb\bar{b}$ ,  $Wc\bar{c}$ ,  $Wc_j$ ,  $Wj_g$ ,  $Wg_g$ , and single top ( $t$ -channel and  $s$ -channel) backgrounds.

The event probabilities are combined into an event probability discriminant:  $EPD = P_{signal} / (P_{signal} + P_{background})$ , where  $P_{signal} = P_{WW} + P_{WZ}$  and  $P_{background} = P_{Wb\bar{b}} + P_{Wc\bar{c}} + P_{Wc_j} + P_{Wj_g} + P_{Wg_g} + P_{st}$ . We make templates of the EPD for all signal and background processes and ultimately extract the signal using a fit of the observed EPD distribution to a sum of the signal and background templates.

Figure 1 shows the dijet mass in bins of EPD. Most of the background events have low EPD, while events with  $EPD > 0.25$  are already very signal-like. The signal-to-background ratio improves with increasing EPD.

Before comparing the observed EPD to the prediction, we validate the Monte Carlo modeling of the quantities that enter the matrix element calculation (the jet and lepton energies and angles). We divide events into three regions according to their  $M_{jj}$ : the signal-rich region with  $55 < M_{jj} < 120$  GeV/ $c^2$  and two control regions with very little expected signal,  $M_{jj} < 55$  GeV/ $c^2$  and  $M_{jj} > 120$  GeV/ $c^2$ . We compare the observed distributions to the predicted distributions in these three regions. In addition to the matrix element input quantities, we also check the modeling of the  $\cancel{E}_T$  and  $m_T(W)$  to validate the description

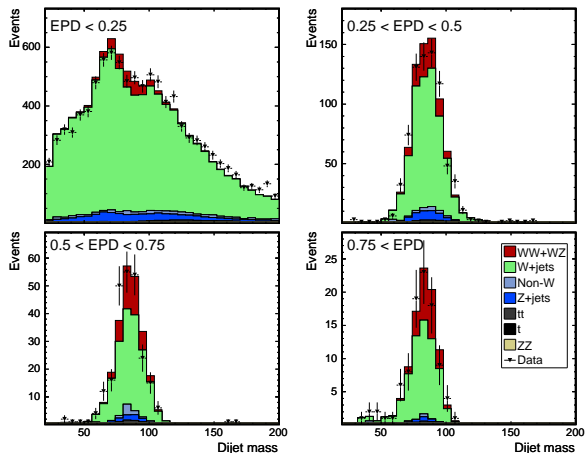


Figure 1:  $M_{JJ}$  for events with  $\text{EPD} < 0.25$  (top left),  $0.25 < \text{EPD} < 0.5$  (top right),  $0.5 < \text{EPD} < 0.75$  (bottom left), and  $\text{EPD} > 0.75$  (bottom right).

of non- $W$  events. Finally we check  $\Delta R_{jj}$ , and  $p_{T,jj}$  to validate the modeling of the correlations between the two jets. All of these quantities are well-described by the simulation for our event selection.

A small discrepancy in the modeling of  $M_{jj}$  itself can be seen when combining the two control regions; it is also visible in the low-EPD region of Fig. 1. We assign a systematic uncertainty on the shape of the EPD in the  $W$ +jets background associated with this discrepancy by reweighting Monte Carlo events to make them agree with data. The weights are derived in the control regions and extrapolated through the signal region to avoid bias from the expected signal. This uncertainty has a negligible effect on the results, because a large fraction of background events lie in the first few bins of the EPD distribution. Small changes in modeling of those background events do not significantly change the shape of the EPD.

## 6. Systematic Uncertainties

In addition to the uncertainty due to the  $M_{jj}$  mis-modeling described above, we consider several other sources of systematic uncertainty, taking into account their effect on both the signal acceptance and the shape of the background and signal templates. The uncertainty on the normalization of the backgrounds is considered part of the statistical uncertainty. The largest systematic uncertainty is due to the jet energy scale (JES) uncertainty. Its effect is quantified by varying the jet energies in the simulated samples by  $\pm 1\sigma$ . We assign both an acceptance uncertainty and a shape uncertainty on the signal templates due to the JES. Other sources of systematic uncertainty considered are initial and final state radiation, parton distribution functions, jet energy resolution, the fac-

torization and renormalization scale ( $Q^2$  scale) used in the ALPGEN  $W/Z$ +jets simulations, and the integrated luminosity.

## 7. Results

The observed and predicted EPDs are shown in Figure 2. We use a binned maximum likelihood fit of the observed EPD to a sum of templates. Systematic uncertainties are incorporated into the fit as nuisance parameters. We perform pseudo-experiments to calculate the probability ( $p$ -value) that the background-only discriminant fluctuates up to the observed result (observed  $p$ -value) and up to the median expected signal plus background result (expected  $p$ -value). We observe a  $p$ -value of  $2.1 \times 10^{-7}$ , corresponding to a signal significance of  $5.4\sigma$ , where  $5.1\sigma$  was expected. The observed  $WW + WZ$  cross section is  $17.7 \pm 3.1(\text{stat}) \pm 2.4(\text{sys})$  pb.

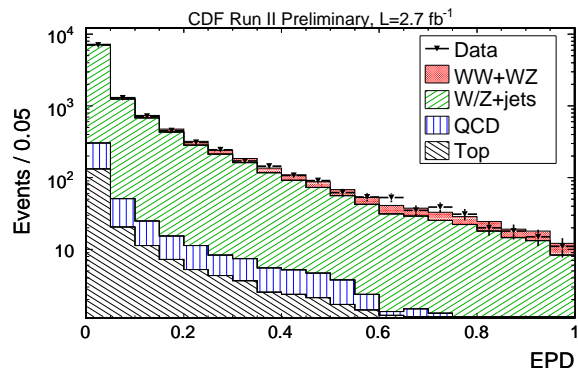


Figure 2: Observed EPD distribution superimposed on expected distribution from simulation.

## 8. Search Using Fit to $M_{jj}$

A complimentary search for a resonance in the invariant mass distribution has been carried out by fitting the  $M_{jj}$  shape to a sum of signal and background templates. The background should be smoothly falling while the signal should exhibit a peak at around 80 GeV from the hadronic decay of a  $W$  or  $Z$  boson. This is a somewhat simpler search technique than using matrix elements as described above, but is not expected to be as sensitive since it does not take advantage of the full event kinematics. A larger data sample was used for this search, corresponding to  $3.9 \text{ fb}^{-1}$  of integrated luminosity.

The event selection for this search is somewhat different than what has been described for the matrix element analysis. The central lepton triggers are used, and offline events are required to contain

one electron candidate with  $E_T > 20\text{GeV}$  or one muon candidate with  $p_T > 20\text{GeV}/c$ . We require  $\cancel{E}_T > 25\text{ GeV}$  and at least two jets with  $E_T > 20\text{ GeV}$ . The non- $W$  background is reduced by requiring  $m_T(W) > 30\text{ GeV}/c^2$ . Events are rejected if the two jets have  $\Delta\eta(J1, J2) > 2.5$ . We also reject events whose hadronic vector boson candidate has  $p_T < 40\text{ GeV}$ ; this selection improves the agreement between data and simulation and ensures a smoothly falling shape in the background dijet invariant mass in the expected signal region.

On data, we estimate the signal fraction by performing a  $\chi^2$  fit to the dijet invariant mass separately for the high  $p_T$  muon and electron samples. Three  $M_{jj}$  template distributions are used in the fit. The first is the combination of  $W$ +jets,  $Z$ +jets,  $t\bar{t}$  and single top production (referred to electroweak (EWK) backgrounds) where the relative normalizations are estimated using predicted cross sections and efficiencies derived from simulation. The overall normalization of the EWK contribution is a free parameter in the signal extraction. The second template is the multi-jet QCD background template; its normalization is constrained by the fit to the  $\cancel{E}_T$  described earlier. The third template describes the signal and its normalization is a free parameter in the fit. In addition, the global normalization of the sum of our signal and background models is a free parameter. Figure 3 shows the data superimposed on the fitted templates after the electron and muon samples are combined.

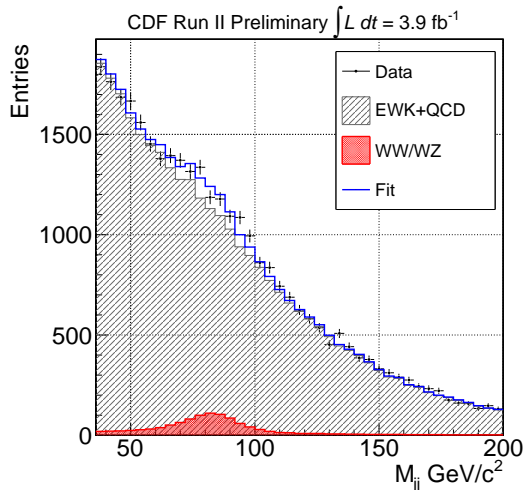


Figure 3: Dijet mass distribution in data superimposed on the predicted background and signal distributions.

The systematic uncertainties in the fit to the  $M_{jj}$  distribution are treated in a similar way as in the matrix element search. In this case, however, the largest sources of systematic uncertainty are the shape uncertainties of the EWK and multi-jet background templates. The jet energy scale uncertainty is also significant, as is the overall 6% uncertainty on the integrated

luminosity.

We estimate  $428 \pm 177$  (stat)  $\pm 56$  (sys) events in the  $WW/WZ \rightarrow e\nu jj$  sample and  $650 \pm 149$  (stat)  $\pm 66$  (sys) events in the  $WW/WZ \rightarrow \mu\nu jj$  sample, giving cross sections of  $10.3 \pm 4.2$  (stat)  $\pm 1.7$  (sys) pb in the electron sample and  $19.5 \pm 4.7$  (stat)  $\pm 2.8$  (sys) pb in the muon sample. Combining the two decays, we estimate a total of  $1079 \pm 232$  (stat)  $\pm 86$  (sys)  $WW/WZ \rightarrow l\nu jj$  events, corresponding to a significance of  $4.6\sigma$  and a cross section of  $\sigma_{WW/WZ+X} = 14.4 \pm 3.1$  (stat)  $\pm 2.2$  (sys) pb. This result agrees with the cross section measured with the matrix element technique as well as with NLO prediction.

## 9. Conclusions

In summary, we have observed  $WW + WZ$  production in the lepton plus two jets final state. We performed two searches: one building a discriminant using matrix element calculations and the other looking for a resonance on top of a smoothly falling dijet mass distribution. The signal was observed with  $5.4\sigma$  significance with the matrix element search, and  $4.6\sigma$  evidence of the signal was found in the  $M_{JJ}$  search. The  $WW + WZ$  cross section was measured to be  $17.7 \pm 3.1$  (stat)  $\pm 2.4$  (sys) pb and  $14.4 \pm 3.1$  (stat)  $\pm 2.2$  (sys) pb with the matrix element and  $M_{JJ}$  searches respectively. These two results are in good agreement with each other and with the NLO prediction of  $16.1 \pm 0.9$  pb.

## Acknowledgments

We thank the Fermilab staff and the technical staffs of the participating institutions for their vital contributions. This work was supported by the U.S. Department of Energy and National Science Foundation; the Italian Istituto Nazionale di Fisica Nucleare; the Ministry of Education, Culture, Sports, Science and Technology of Japan; the Natural Sciences and Engineering Research Council of Canada; the Humboldt Foundation, the National Science Council of the Republic of China; the Swiss National Science Foundation; the A.P. Sloan Foundation; the Bundesministerium für Bildung und Forschung, Germany; the Korean Science and Engineering Foundation and the Korean Research Foundation; the Science and Technology Facilities Council and the Royal Society, UK; the Institut National de Physique Nucleaire et Physique des Particules/CNRS; the Russian Foundation for Basic Research; the Ministerio de Ciencia e Innovación, and Programa Consolider-Ingenio 2010, Spain; the Slovak R&D Agency; and the Academy of Finland.

## References

- [1] K. Hagiwara, S. Ishihara, R. Szalapski, and D. Zeppenfeld, *Phys. Rev. D* **48**, 2182 (1993).
- [2] CDF Collaboration: D. Acosta *et al.*, *Phys. Rev. Lett.* **94**, 211801 (2005); A. Abulencia *et al.*, *ibid* **98**, 161801 (2007).
- [3] D0 Collaboration: V.M. Abazov *et al.*, *Phys. Rev. Lett.* **94**, 151801 (2005); *Phys. Rev. D* **76**, 111104(R) (2007).
- [4] t. Aaltonen *et al.* (CDF Collaboration), *Phys. Rev. Lett.* **103**, 091803 (2009).
- [5] V. M. Abazov *et al.* (D0 Collaboration), *Phys. Rev. Lett.* **102**, 161801 (2009).
- [6] T. Aaltonen *et al.* (CDF Collaboration), *Phys. Rev. Lett.* **103**, 101802 (2009).
- [7] T. Acosta *et al.* (CDF Collaboration), *Phys. Rev. D* **71**, 032001 (2005).
- [8] T. Sjöstrand *et al.*, *Comput. Phys. Commun.*, **135**, 238 (2001).
- [9] M. L. Mangano *et al.*, *J. High Energy Phys* **0307**, 001 (2003)
- [10] J. Alwall *et al.*, *J. High Energy Phys.* 09 (2007) 028.
- [11] J. Pumplin *et al.*, *J. High Energy Phys.* **0207**, 012 (2002).
- [12] F. Maltoni and T. Stelzer, *J. High Energy Phys.* **0302**, 027 (2003).